Continuous-wave fiber cavity ring-down magnetic field sensing method based on frequency-shifted interferometry

Hui Tian (田 辉)[1,2], Ciming Zhou (周次明)[1,3*], Dian Fan (范 典)[1,3], Yiwen Ou (欧艺文)[1,3], and Dijia Yin (尹嘉笛)[1,3]

[1]*National Engineering Laboratory for Fiber Optic Sensing Technology, Wuhan University of Technology, Wuhan 430070, China*

[2]*School of Science, Wuhan University of Technology, Wuhan 430070, China*

[3]*Key Laboratory of Fiber Optic Sensing Technology and Information Processing, Ministry of Education, Wuhan University of Technology, Wuhan 430070, China*

[*]*Corresponding author: zcm@whut.edu.cn*

Received July 4, 2014; accepted October 11, 2014; posted online November 20, 2014

We demonstrate a novel all-fiber cavity ring-down (CRD) magnetic field sensing method that uses frequency-shifted interferometry, and does not require any optical pulse and fast electronics compared with conventional CRD schemes. The sensing element in the ring-down cavity is a fiber taper surrounded by magnetic fluid, whose refractive index varies as an external magnetic field is applied. Magnetic field strength measurement is successfully achieved within a range from 8 to 850 Gs. A resolution of 0.00105 ± 0.00003 dB/Gs is obtained in the approximately linear segment from 423.2 to 766.6 Gs. The sensing method is potential for sensing other physical and chemical parameters.

OCIS codes: 060.2370, 060.4370, 070.4340, 160.4670.

doi: 10.3788/COL201412.120604.

Ever since conventional cavity ring-down (CRD) techniques were first proposed in 1984 by Anderson *et al.*[1], who used CRD techniques to measure mirror reflectivity, CRD has been developed to be a sensitive and powerful technique to detect weak optical losses[2–4]. Unlike conventional direct measurement schemes in which the attenuation of transmitted light through a sample is measured, CRD techniques measure the ring-down time of the cavity instead of the intensity decrease with absorption length and concentration. The absorption loss introduced by a sample in the CRD cavity can be derived from the measured CRD time[5]. The higher the absorption, the shorter is the CRD time. Proportional to the loss in the cavity, the ring-down time is independent of excitation intensity, and this results in a low susceptibility to laser noise and immunity to external loss contributions. As a result, the signal to noise ratio of CRD is enhanced[6,7]. The attenuation coefficient of the absorption sample can be derived. However, pulsed light that is usually generated by modulation of a continuous-wave (CW) laser used in CRD requires a narrow linewidth and a high-speed detector. To avoid utilizing pulsed light, CW light as the source in a frequency-shifted interferometry (FSI) CRD technique proposed by Qian *et al.*[8,9]. This technique is different from phase-shifted (PS) CRD[10] and time domain CRD[5,6]. In PS-CRD, an intensity modulation is applied to the input light so as to produce a phase shift related to the temporal decay time constant[11], whereas in FSI-CRD, frequency modulation produces an interferogram which contains light intensity decay information as a function of the distance traveled. A Fourier transform (FT) is carried out to obtain the familiar temporal decay curves. In time domain CRD, light intensity decay information is closely related to real-time signal. Only by recording CRD time, the cavity loss can be obtained. However, in FSI-CRD, the cavity loss was only revealed from the FT of the frequency-modulated CW interference signal exiting from a ring-down cavity. The deduction of cavity loss in FSI-CRD is equal to processing the relationship between the intensity decay and the distance traveled by light. A cavity optomechanical magnetometer based on a magnetostrictive material and an optical microresonator was proposed by Forstner *et al.* and a sensitivity of 400 nT $\mathrm{Hz}^{-1/2}$ was achieved[12]. A magnetic field sensor configured as a core–cladding–mode interferometer by incorporating magnetic fluid (MF) was proposed and the sensitivity reached ~16.206 pm/Gs ranging from 0 to 214 Gs[13]. If sensing elements, such as long-period gratings[14] or fiber tapers[15,16], are inserted in the cavity, as customary in the conventional CRD techniques, many physical or chemical quantities[17,18] that affect the intensity of the light inside the FSI-CRD cavity can be detected by this method.

In this letter, we report a novel magnetic field sensing method based on FSI-CRD with a CW source, a high-gain balanced photodetector, an acousto-optic modulator (AOM), and a data acquisition card (DAQ). The magnetic field sensing method is verified by experiments with the use of a type of MF as the sensing material inside the fiber CRD cavity. The tunable refractive index characteristics of MF, as a kind of the

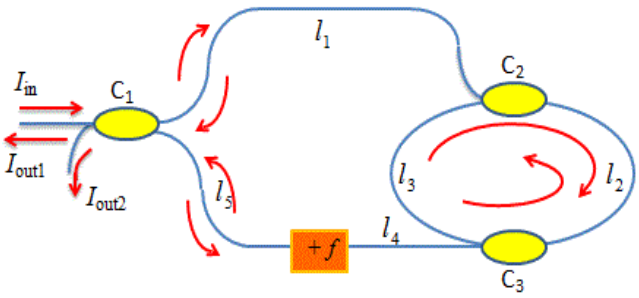

Fig. 1. FSI with a fiber ring-down cavity[8].

sensitive medium[19–21], are applied in this letter. The results show that this novel method based on FSI can be applicable for detecting current and magnetic field intensities. As a result, a stable relationship between cavity loss and magnetic field ranging from 8 to 850 Gs is obtained.

The FSI technique was proposed by Qian *et al.*, and its comprehensive description was provided in Refs. [8,9]; the technique is similar to a frequency-shifted fiber Signac loop. As shown in Fig. 1[8], CW light with a frequency v separates into two beams after traveling across the coupler C_1. One beam in path l_5 is frequency shifted by an amount of $+f$ after it passes through a frequency shifter, and the other beam in path l_1 will oscillate with its original frequency v. The two components continue to propagate into the cavity through couplers C_2 and C_3, respectively, and then circulate in the ring-down cavity. After each trip in the cavity, one fraction of the modes propagating in clockwise and anticlockwise directions leaks out of the cavity and reaches the coupler C_1. They may interfere if they arrive at the same time after they have traveled the same number of round trips in the cavity. The leaked mode fraction in the clockwise direction is also frequency shifted by an amount of $+f$ while it passes through the frequency shifter. Therefore, the two fractions of light have the same frequency $v+f$ (Table 1). Because field components E_{2m} are shifted earlier than E_{1m}, the two fractions of light interfere at coupler C_1 and show a phase difference $\Delta\varphi$[8,9], whereas the coherence length of the light source is shorter than the fiber cavity length d. The detailed transmission path is shown in Table 1, where m ($m = 0$, 1, 2, ...) is the number of light round trips in the cavity, and $d = l_1 + l_3$(~53m) is the cavity length.

$$\Delta\varphi = 2\pi \frac{n\left[l_1 + l_2 + m(l_2 + l_3) + l_4 - l_5\right]}{c} f. \tag{1}$$

The differential output signal ΔI[8,9,22] (shown in Eq. (1)) is a cosine function of f, and this cosine function oscillates at a frequency $F_m = n(md+l)/c$ related to both the distance $L = md$ in the ring-down cavity and the asymmetry of two arms of the Mach–Zehnder interferometer: $l = l_1+l_2+l_4-l_5$.

$$\Delta I \propto \sum_{m=0}^{\infty} I_m \cos\left(\Delta\varphi\right) = \sum_{m=0}^{\infty} I_m \cos\left[2\pi \frac{n\left(md + l\right)}{c} f\right]$$
$$= \sum_{m=0}^{\infty} I_m \cos\left(2\pi F_m f\right). \tag{2}$$

In Eq. (1), n is the effective mode index of the fiber, c is the speed of light, and l_i ($i = 1, 2, 3, 4, 5$) is the fiber length defined in Fig. 1. I_m is the amplitude proportional to the interfering light intensity after m cavity round trips, and each cosine component corresponds to the interference of the light that has traveled through the fiber cavity for m round trips.

We take the FT of ΔI to resolve the distance that the light has traveled in the cavity from the oscillation frequency components $F_m \cdot F_m$ is unique for each round-trip number m and is equally spaced by nd/c. A series of I_m[8,9,22] exponentially decreases as light passes the sensing element in the cavity. If the attenuation coefficients are recorded in different magnetic fields, we can deduce the cavity loss. Therefore

$$I_m = I' \exp\left[-\left(\alpha - \log\kappa_c\right)m\right] = I' \exp\left[-\left(\alpha - \log\kappa_c\right)\frac{L}{d}\right], \tag{3}$$

$$\delta_{\text{loss}} = 4.34\alpha = 4.34\left(\frac{d}{t_1} + \log\kappa_c\right), \tag{4}$$

where κ_c is the loss inherent to the cavity setup, which includes the background cavity loss of an empty ring-down cavity, splices loss, fiber scattering loss, fiber absorption loss in the cavity sections l_2 and l_3, fiber couplers insertion loss of C_2 and C_3, and attenuator loss. t_1 is the attenuation coefficient of exponential function. α is the sensing element transmission attenuation, which depends on the refractive index of the MF[19–21] because of evanescent field absorption. Since the effect

Table 1. Field Components Arriving at C_1 After Round Trips in the Ring-down Cavity

Field Components	Path Followed	Frequency upon Returning to C_1
E_{1m}	$C_1 \rightarrow l_1 \rightarrow l_2+md \rightarrow C_3 \rightarrow l_4 \rightarrow$ AOM $\rightarrow l_5 \rightarrow C_1$	$v+f$
E_{2m}	$C_1 \rightarrow l_5 \rightarrow$ AOM $\rightarrow l_4 \rightarrow C_3 \rightarrow l_2+md \rightarrow l_1 \rightarrow C_1$	$v+f$

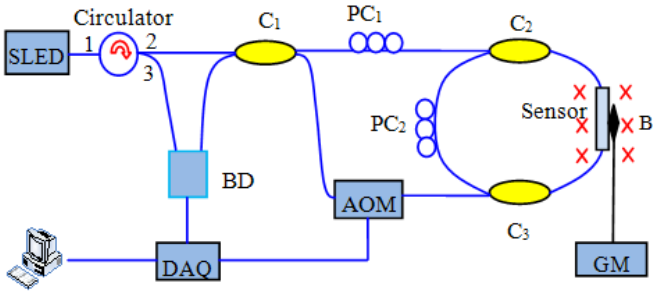

Fig. 2. Experimental system based on FSI-CRD. C_1, 50/50 fiber coupler; C_2 and C_3, 0.5 and 99.5 fiber couplers; BD, balanced detector; PC_1 and PC_2, polarization controllers; GM, gaussmeter.

of temperature to MF refractive index is weak[19], we ignore the impact of the temperature in our experiment.

The experimental system is shown in Fig. 2. A superluminescent light-emitting diode source (44 nm bandwidth with a central wavelength of 1550 nm) was set to 5 mW at 1550 nm, and the light separated into two components at C_1 after it passed through the circulator (its three direction ports are shown in Fig. 2). The differential interference voltage signal was digitized by a 100 KSs^{-1}, 16-bit USB multi-channel DAQ card (USB-6361 National Instruments, Austin, TX, USA), which was triggered by AOM for synchronization. A custom LabVIEW program was used to control the AOM (AMM-100-20-25-1550-2FP BRIMROSE) linearly sweeping from 90 to 110 MHz at step of 0.01 MHz with a 1 ms duration and fitted the peaks of the intensity signal. The fitting results were averaged and stored for further processing. A high-gain balanced photodetector (New Focus 2117, 10 MHz bandwidth, >107 V/W gain) was used to attain photoelectric conversion, with a gain of 34.78 dB. The linear polarization states of the two interfering beams fluctuated due to the polarization drift[23]. Two linear polarization controllers (three paddles) were used to maintain a preferable interference phenomenon. Due to pressure, strain and birefringence

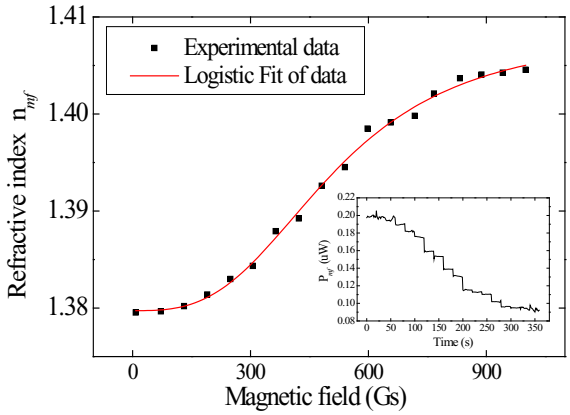

Fig. 3. Refractive index n_{mf} as a function of magnetic field. The inset shows the measured reflected powers P_{mf} in real time for various magnetic field strengths.

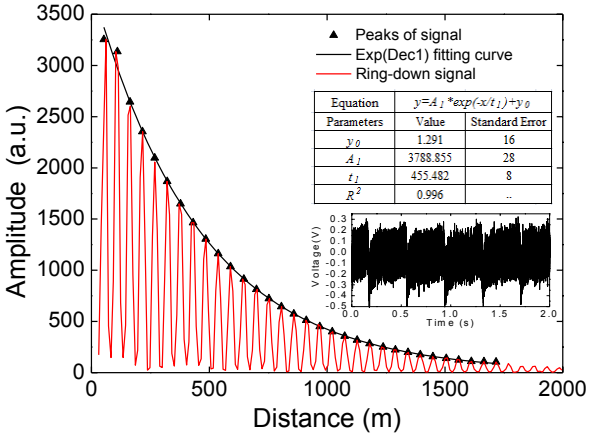

Fig. 4. Typical fiber CRD transient measured by FSI-CRD system at a current of 0.35 A. The inset is the raw interferogram of the measurement.

would affect the polarization states of the interfering beams and to avoid these disturbances we fixed the ring-down cavity and the sensing device on a hover platform. In addition, a stable and favorable environment would enhance the accuracy of measurement and the sensitivity of the sensor.

We prepared a section of 30 mm long SMF-28 fiber and etched it in the hydrofluoric acid solution at the concentration of 25% for approximately 2.5 h. The fiber taper (18 μm diameter) was then immersed in MF (EMG Series Water-based Ferrofluid, Ferrotec, USA), which was composed of Fe_3O_4 nanoparticles, water soluble dispersant, and water with volume 3.2%, 17.6%, and 79.2%, respectively. The effective refractive index of MF varied with the change in magnetic field strength since Fe_3O_4 particles in the MF agglomerated and formed a long-chain structure parallel to the field direction with the increment of magnetic field strength[19–21]. To obtain the quantitative information between the refractive index of the MF and magnetic field intensity, the method reported in Ref. [24] was employed and the results are shown in Fig. 3. The inset shows the measured reflected powers P_{mf} in real time for various magnetic field strengths when the detecting fiber tip is immersed in the MF. P_{air} = 8.149 μW and P_{water} = 0.660 μW were the measured reflected powers when the detecting fiber tip was placed in air and immersed in water, respectively. The central wavelength of the ASE light used was 1310 nm and the working temperature was 27 °C. From Fig. 3, it can be seen that the refractive index increased monotonously from 1.3830 to 1.4037 as the field strength rose from 300 to 750 Gs, and then it almost remained unchanged as the field strength was more than 800 Gs.

Therefore, the intensity of light that passed through the sensing element decreased as a result of evanescent field absorption. The cylindrically symmetrical magnetic field was changed by adjusting the passing current through a pair of coaxial ferromagnetic coils, and

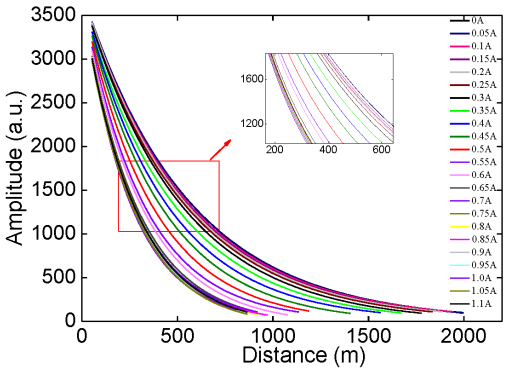

Fig. 5. Change in the exponential decay curve with current from 0 to 1.1 A.

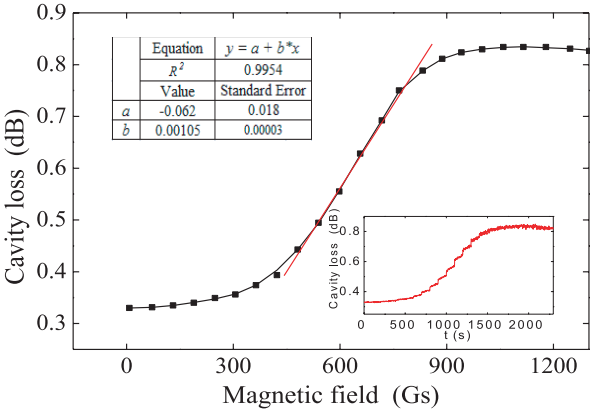

Fig. 6. Relationship between magnetic field intensity and cavity loss. The inset (50 points/0.05 A) shows the real-time cavity loss.

a gaussmeter (Lake Shore 460) was fixed beside the sensor in the center of the uniform field zone. The FSI-CRD system was set to record the value of cavity loss every 2 s. The current was varied from 0 to 1.10 A at the step of 0.05 A, with a 100 s duration for each current setting. A typical ring-down measurement at a current of 0.35 A is shown in Fig. 4 after the interference signal (the inset in Fig. 4 at the balanced detector was operated by FT with a transform size of 2^{20}). From the attenuation coefficient t_1 in the graph by fitting the first 30 peaks of amplitude with an exponential function, the calculated cavity loss in the loop was 0.4004 ± 0.0002 dB from Eq. (4). The correlation coefficient R^2 of the exponential fitting was always larger than 0.998 in the following experiments. When the current was 0 A, the cavity loss was 0.3299 dB per round trip. Figure 5 shows the exponential decay curves with different currents, from which different magnetic fields (Table 2) were deduced. Each decay curve is obtained according to the method shown in Fig. 4 and yields a value of cavity loss (inset of Fig. 6).

In Fig. 6, the curve is a smoothed line splicing the data points, and the straight line is a linear fit. At the beginning of the magnetic field, the cavity loss has a slow change with magnetic field from 0 to 300 Gs in Fig. 6, which indicates the threshold magnetic field of 300 Gs. Then the cavity loss is gradually increased and has an approximately linear range from 423.2 to 766.6 Gs. A linear fitting is illustrated in Fig. 6, while resolution of 0.00105 ± 0.00003 dB/Gs is obtained in the linear segment, and the correlation coefficient R^2 of the linear fitting is 0.995. When the magnetic field intensity is greater than 850 Gs, the sensing system is saturated due to the magnetization saturation. The variation trend of the cavity loss is almost consistent with the features of MF refractive index under magnetic field in Fig. 3. Because the measured data are obtained in different principles and experimental setups, there is a slight difference between the linear range in Fig. 3 and that of in Fig. 6. The real-time change of cavity loss with the increase in current can be clearly observed from the rising steps in the inset of Fig. 6.

In conclusion, we establish a FSI-CRD magnetic field sensing method. The FSI technique is used to transfer the distance traveled by the continuous lightwave into the frequency domain by the FT. The results are not affected by the intensity fluctuation of the CW light. Optical pulses and high-speed detections as in conventional CRD system are therefore avoided. The cavity loss can be deduced from the rate of decay in the amplitude–frequency curve. The sensing method is verified by experiments with the use of a type of MF as the sensing material inside the fiber CRD. A stable relationship between cavity loss and magnetic field is shown from 0 to 850 Gs. The experimental results achieve a resolution of 0.00105 ± 0.00003 dB/Gs in the approximately linear segment from 423.2 to 766.6 Gs. Therefore, this sensing method indicates a promising potential for other physical or chemical sensing if other kinds of optical fiber sensing elements are employed inside the fiber CRD.

This work was supported by the Project of National Science Foundation of China (Nos. 61077061 and 61377091) and the Fundamental Research Funds for the Central Universities (Nos. WUT 2013-II-023 and WUT 2014-zy-115).

Table 2. Relationship Between Current and Magnetic Field Beside the Sensor

Current (A)	0	0.05	0.1	0.15	0.2	0.25	0.3	0.35	0.4	0.45	0.5	0.55	0.6	0.65	0.7	0.75	0.8	0.85	0.9	0.95	1.0	1.05	1.1
Magnetic Field (Gs)	8	72	131	190	249	306	364	423	481	540	598	657	718	767	833	888	942	1000	1059	1116	1179	1247	1301

References

1. D. Z. Anderson, J. C. Frisch, and C. S. Masser, Appl. Opt. **23,** 1238 (1984).
2. J. J. Scherer, J. B. Paul, A. O'Keefe, and R. J. Saykally, Chem. Rev. **97,** 25 (1997).
3. G. Berden and R. Engeln, *Cavity Ring-down Spectroscopy: Techniques and Applications* (Wiley-Blackwell, 2009).
4. B. Li, Z. Qu, Y. Han, L. Gao, and L. Li, Chin. Opt. Lett. **8,** 94 (2010).
5. D. Fan, J. Gong, and A. B. Wang, Proc. SPIE **8421,** 842160 (2012).
6. N. Ni, C. C. Chan, L. Xia, and P. Shum, IEEE Photon. Technol. Lett. **20,** 1351 (2008).
7. J. Y. Lee, J. W. Kim, Y. S. Yoo, J. W. Hahn, and H. W. Lee, Appl. Phys. **91,** 581 (2002).
8. F. Ye, L. Qian, and B. Qi, Opt. Lett. **36,** 2080 (2011).
9. F. Ye, L. Qian, and B. Qi, J. Lightwave Technol. **27,** 5356 (2009).
10. R. Engeln, G. V. Helden, and G. Meijer, Chem. Phys. Lett. **262,** 105 (1996).
11. Z. Tong, A. Wright, T. McCormick, R. Li, R. D. Oleschuk, and H. P. Loock, Anal. Chem. **76,** 6594 (2004).
12. S. Forstner, S. Prams, J. Knittel, E. D. van Ooijen, J. D. Swaim, G. I. Harris, A. Szorkovszky, W. P. Bowen, and H. Rubinsztein-Dunlop, Phys. Rev. Lett. **108,** 120801 (2012).
13. M. Deng, D. H. Liu, and D. C. Li, Sens Actuators A **211,** 55 (2014).
14. S. Pu and X. Gu, Opt. Lett. **34,** 1774 (2009).
15. Y. Yu, L. Jiang, B. Li, Z. Cao, and S. Wang, Chin. Opt. Lett. **11,** 110603 (2013).
16. P. B. Tarsa, A. D. Wist, P. Rabinowitz, and K. K. Lehmann, Appl. Phys. Lett. **85,** 4523 (2004).
17. H. Waechter, J. Litman, A. H. Cheung, J. A. Barnes, and H. Loock, Sensors **10,** 1716 (2010).
18. G. Stewart, K. Atherton, H. Yu, and B. Culshaw, Meas. Sci. Technol. **12,** 843 (2001).
19. Y. Zhao, D. Wu, R. Q. Lv, and Y. Ying, IEEE Trans. Magn. **99,** 1 (2014).
20. T. Hu, Y. Zhao, X. Li, J. Chen, and Z. Lv, Chin. Opt. Lett. **8,** 392 (2010).
21. J. Zheng, X. Dong, P. Zu, L. Shao, C. Chan, Y. Cui, and P. Shum, Opt. Express **21,** 17863 (2013).
22. F. Ye, C. M. Zhou, B. Qi, and L. Qian, Sens. Actuators B: Chem. **184,** 150 (2013).
23. A. Yariv and P. Yeh, *Photonics*: *Optical Electronics in Modern Communication* (Oxford University Press, 2007).
24. S. Pu, X. Chen, Y. Chen, W. Liao, L. Chen, and Y. Xia, Appl. Phys. Lett. **86,** 171904 (2005).